Vacuum-Processed Small Molecule Organic Photodetectors with Low Dark Current Density and Strong Response to Near-Infrared Wavelength

by Richie Estrada

Submission date: 17-Apr-2023 01:49AM (UTC+0700)
Submission ID: 2066066963
File name: 7_10.1002_adom.202000519.pdf (2.8M)
Word count: 7245
Character count: 34629

ADVANCED OPTICAL MATERIALS
www.advopticalmat.de

Vacuum-Processed Small Molecule Organic Photodetectors with Low Dark Current Density and Strong Response to Near-Infrared Wavelength

Chih-Chien Lee, Richie Estrada, Ya-Ze Li, Sajal Biring, Nurul Ridho Al Amin, Meng-Zhen Li, Shun-Wei Liu, and Ken-Tsung Wong**

A near-infrared photodetector with optimized performance is reported using varied thickness (20, 40, 60, and 80 nm) of the active layer comprising chloroaluminium phthalocyanine (ClAlPc) and fullerene (C_{70}) at the ratio of 1:3, and TAPC:10% MoO_3 and BPhen as electron and hole blocking layers, respectively. The experimental results reveal that the photodetector with 80 nm thick active layer provides the best performance at the wavelength of 730 nm achieving a very low dark current density of 1.15×10^{-9} A cm^{-2} and an external quantum efficiency of 74.6% with a responsivity of 0.439 A W^{-1} at −2 V bias. Additionally, the device exhibits a dramatic high detectivity of 4.14×10^{13} cm Hz$^{1/2}$ W^{-1} at 0 V bias. The device exhibits not only a large linear response over a wide optical power range (LDR of 173.0 dB), but also a broad frequency response (778.7 kHz) and rise/fall time of 2.13/0.77 µs (based on trigger pulses at a frequency of 10 kHz) at the applied bias of −2 V. Based on the impedance spectroscopic study and the conventional characterization of electro-optical properties, the results demonstrate the superiority of this device over other small molecule-based near-infrared photodetectors.

1. Introduction

Organic semiconductors have found enormous applications in organic electronics which encompass organic light-emitting diodes (OLEDs), organic photovoltaics (OPVs), organic photodetectors (OPDs), biological sensors, and so on.[1,2] Currently, a boost in research works on OPDs have been observed after the successful commercialization of OLEDs and OPVs, since photodetectors can be widely applied in various fields such as imaging, optical communication, environmental/health monitoring, night vision, and chemical/biological sensing.[2–17] Although OPDs show tremendous potentials, yet certain key parameters such as external quantum efficiency (EQE), linear dynamic range (LDR), and transient response should be improved significantly to optimize the detectivity so that it can vie against its inorganic counterpart.[5,14,15,18–22] The EQE of an OPD device is typically expressed in percentage that reflects the number of electrons collected at the electrode per incident photon at specific wavelength, while LDR describes the maximum dynamic range of an OPD device corresponding to its linear response in relation with the variation of incident light intensities.[19,20] The collection/extraction efficiencies of the photogenerated charge carriers are generally studied by the transient response of the OPDs.[13–15] On the other hand, detectivity of an OPD device is predominantly limited by the noise, which can be improved generally by inserting carrier blocking layers to suppress undesired charge injection from the electrodes as well as to facilitate the charge collection by the electrodes simultaneously.[11]

Both the polymer- and small molecule-based organic semiconductors have been studied to demonstrate a broad-band and narrow-band NIR photodetectors with high-performance successfully.[23] Significant research works have been conducted mostly on polymer-based OPDs due to the broader optical absorption compared to small molecules. Recently, Sun et al. reported an efficient polymer solar cell with power conversion efficiency exceeding 16% and optical absorption extended to the NIR region, which is promising for the progress of NIR photodetector.[24] For small molecule-based OPVs, phthalocyanine (Pc) is widely used as a donor material in the absorption's

Prof. C.-C. Lee, R. Estrada, Y.-Z. Li, N. R. A. Amin, M.-Z. Li
Department of Electronic Engineering
National Taiwan University of Science and Technology
Taipei 10607, Taiwan

R. Estrada, Y.-Z. Li, Prof. S. Biring, N. R. A. Amin, M.-Z. Li, Prof. S.-W. Liu
Organic Electronics Research Center
Ming Chi University of Technology
New Taipei City 24301, Taiwan
E-mail: swliu@mail.mcut.edu.tw

Prof. S. Biring, Prof. S.-W. Liu
Department of Electronic Engineering
Ming Chi University of Technology
New Taipei City 24301, Taiwan

Prof. K.-T. Wong
Department of Chemistry
National Taiwan University
Taipei 10617, Taiwan
E-mail: kenwong@ntu.edu.tw

Prof. K.-T. Wong
Institute of Atomic and Molecular Science
Academia Sinica
Taipei 10617, Taiwan

The ORCID identification number(s) for the author(s) of this article can be found under https://doi.org/10.1002/adom.202000519.

DOI: 10.1002/adom.202000519

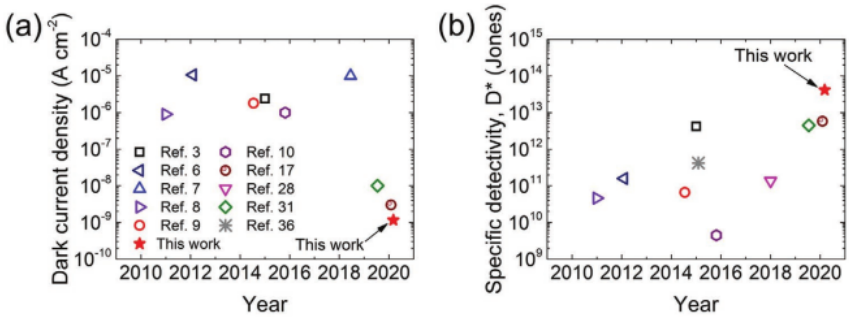

Figure 1. The state-of-the-art of small molecule-based NIR OPDs reported for the last 10 years. The electrical characteristics of a) dark current density (the applied bias voltage of −2 V) and b) the specific detectivity (D^*) for OPDs. Note that the values of D^* were recorded at the absorption wavelength of ≈730 nm.

active layer, e.g., copper (II) phthalocyanine (CuPc), boron subphthalocyanine chloride (SubPc), lead (II) phthalocyanine (PbPc), and chloroaluminium phthalocyanine (ClAlPc).[17,25] An OPD device made with CuPc:C_{60} blend showed the incident photon-to-current efficiency (IPCE) of 51.7% at a wavelength of 620 nm with a specific detectivity of 4.0×10^{11} cm Hz$^{1/2}$ W^{-1} as reported by Higashi et al.[26] The thickness of the active layer plays a vital role in the optimization of optical field distribution, which was studied by Lee et al. demonstrating the change in spectral profile of EQE with the change in the acceptor (C_{70}) thickness of the active layer based on SubPc:C_{70} blend.[27] On the other hand, the range of optical absorption can be extended to 1100 nm by employing PbPc:C_{70} blend as the active layer as mentioned by several studies. For example, Su et al. fabricated an OPD device with PbPc:C_{70} blend as the active layer exhibiting broad-band response in the wavelength range of 300–1100 nm and the EQE of ≈30.2% in the NIR region (at a wavelength of 890 nm).[3] Meanwhile, Choi et al. developed a PbPc-based inverted OPD device demonstrating the dark current density of ≈10^{-6} A cm^{-2} and EQE of 31.1% at a wavelength of 970 nm, and 244 mA W^{-1} and 1.36×10^{11} cm Hz$^{1/2}$ W^{-1} for a respective parameter of responsivity and specific detectivity measured at a bias voltage of −3 V.[28] Another Pc-derivative material, ClAlPc, also shows strong optical absorption in the NIR region with a narrow-band covering from 650 to 750 nm as compared to that of other Pc materials, such as PbPc, zinc phthalocyanine, and tin naphthalocyanine.[4,17,25,29,30] Joo et al. has demonstrated another Pc-based NIR absorber, chloroindium phthalocyanine (ClInPc) blended with C_{60} as the active layer, which achieved a dark current density of ≈10^{-8} A cm^{-2}, EQE > 80% (at a wavelength of ≈705 nm), specific detectivity of 4.5×10^{12} Jones, LDR of 77.2 dB, and frequency response of 2.85 kHz.[31] Note that several research teams highlighted that the active layer composed of ClAlPc as a donor and the fullerene as an acceptor is a promising photovoltaic layer to improve detection ability in the NIR region exploiting the high absorption coefficient (> 1×10^5 cm^{-1}) of ClAlPc in the wavelength range of 615–815 nm.[32–35] Besides, another study by Du et al. reported that the organic phototransistors with ClAlPc/C_{60} heterojunction showed the responsivity of 2.65 A W^{-1} and specific detectivity of 4.2×10^{11} cm Hz$^{1/2}$ W^{-1} at the wavelength of 808 nm.[36]

In the previous works as mentioned above, we have observed that the big challenge is the high dark current density (leakage current) of NIR OPDs. It is because such a parameter is one of the key issues to determine the image sensor's quality. To suppress the OPD's dark current density, inserting a proper carrier blocking layer between the active layer and electrode is a straightforward solution. For example, insertion of the buffer layers of 4,4′-cyclohexylidenebis[*N*,*N*-bis(4-methylphenyl)benzenamine] (TAPC):MoO_3 (ITO side) and BPhen (metal electrode side) for the OPDs can achieve the dark current density of < 1.11×10^{-9} A cm^{-2}.[21] Therefore, we propose an efficient NIR OPDs using the active layer of ClAlPc:C_{70} and suitable carrier blocking layers (TAPC:10% MoO_3 and BPhen) to achieve a wide absorption range of 300–800 nm. In this work, the active layers with a varied thickness (20, 40, 60, and 80 nm) were investigated by using the optical and electrical characterizations, such as dark/light current density, the EQE bias, detectivity, photoresponse (LDR, −3 dB, and rise/fall time), and impedance spectroscopy in details. The optimal device (selected by the highest EQE at −2 V) with 80 nm thick ClAlPc:C_{70} (1:3) blend offers the dark current density of 1.15×10^{-9} A cm^{-2} at −2 V and a specific detectivity of 4.14×10^{13} cm Hz$^{1/2}$ W^{-1} at 0 V under the wavelength of 730 nm, representing the best small molecule-based NIR OPD device ever reported (see **Figure 1**).

2. Results and Discussion

Figure 2a shows the device configuration, molecular structures, and energy level of the respective material. In this study, the OPD devices were composed of the active layer of ClAlPc:C_{70} (1:3) blend sandwiched between the carrier blocking layers and electrodes similar to the general device structure of an OPV.[11,37] The blocking layers act to facilitate charge transfer and inhibit the charge injection under forward and reverse biases, respectively.[38] The better performance of an OPD device relies on minimizing the leakage currents under reverse bias, which is, in general, controlled by the energy barrier for electrons formed at the anode (4.8 eV) and LUMO level (4.3 eV) of the acceptor materials, C_{70}, as well as for holes formed at the cathode (4.2 eV) and HOMO level (5.4 eV) of ClAlPc. Therefore, to improve the energy barriers at the electrodes for further suppression of

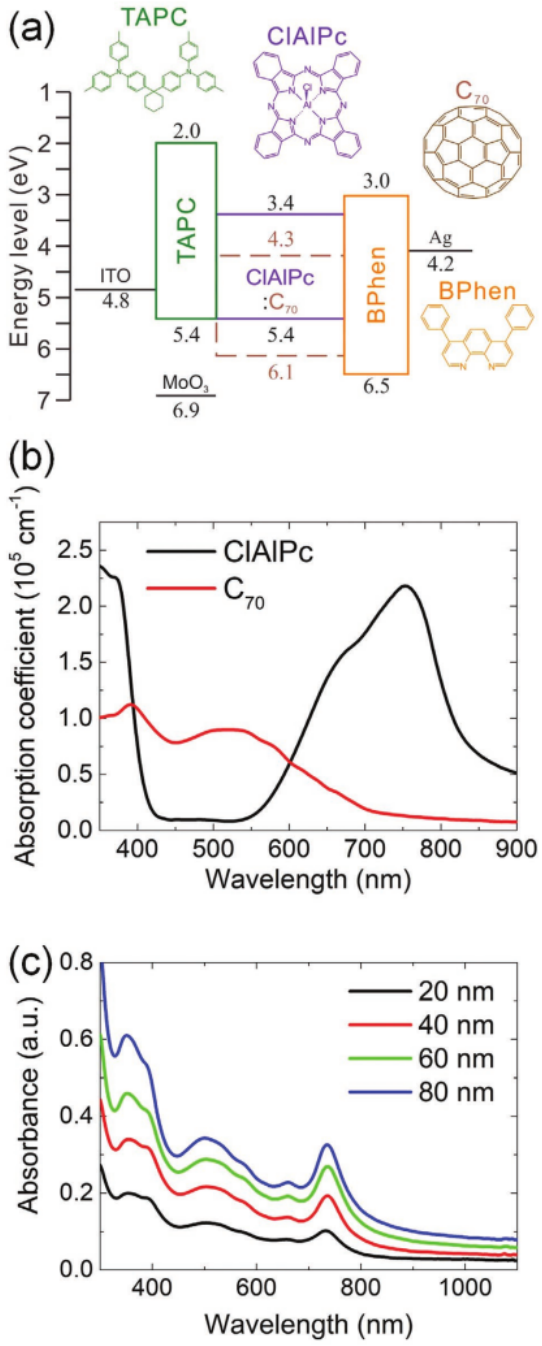

Figure 2. a) The device configuration, molecular structure, and energy level of the respective materials. b) The absorption coefficient of the organic ClAlPc and C_{70} thin-films deposited on a quartz substrate. c) The absorbance spectra of the thin film of ClAlPc:C_{70} (1:3) blends as a function of thickness.

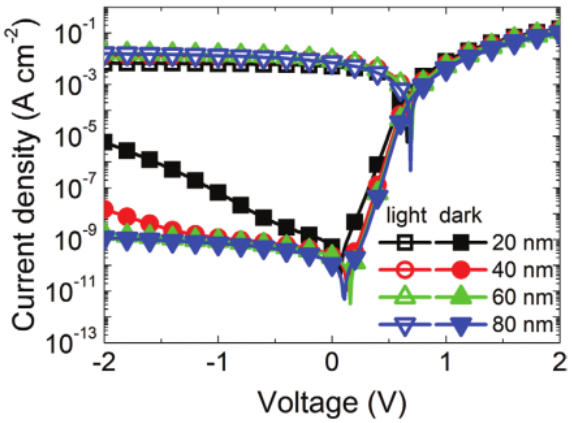

Figure 3. Current density–voltage characteristics (dark and illumination condition) of the OPD devices based on ClAlPc:C_{70} (1:3) blend with various thickness studied in this work.

leakage currents, carrier blocking layers of TAPC:10% MoO_3 (LUMO = 2.0 eV) for electrons and BPhen (HOMO = 6.5 eV) for holes with the thicknesses of 30 nm and 3 nm, respectively, were inserted between the active layer and the corresponding electrodes.[21] Figure 2b shows the absorption coefficient spectra of the respective organic thin-films of ClAlPc and C_{70}, exhibiting strong absorption in the region of ultraviolet to visible light (from < 350 to ≈600 nm) and red to NIR light (from ≈650 to ≈800 nm), respectively. Therefore, a broad-band spectrum with strong absorption extending to NIR could be achieved by blending the active materials with different ratios of 1:5, 1:3, 1:1, 2:1, and 0:1 of donor (ClAlPc) and acceptor (C_{70}) (see Figure S1, Supporting Information). However, the active layer with a blending ratio of 1:3 of ClAlPc:C_{70} shows the optimized photodetection with broad-band absorption from the region of ultraviolet up to NIR light. As a consequence, all the OPD devices under study were fabricated with the active layer of ClAlPc:C_{70} blended at the ratio of 1:3. The performance of OPD device was optimized by tuning the thickness (20, 40, 60, and 80 nm) of the active layer. The absorbance spectra of active layer as a function of the thickness (20, 40, 60, and 80 nm) is presented in Figure 2c for comparison.

Figure 3 shows the current density-voltage characteristics for the OPD device with the active layer thickness of 20, 40, 60, and 80 nm measured under dark and illumination conditions by sweeping bias from the region of 2 to −2 V. It is obvious that the OPD device with the active layer thickness of 20 nm shows a high leakage current (5.9×10^{-6} A cm^{-2}) at a bias voltage of −2 V as compared to that of the OPD device with the active layer thickness of 80 nm (1.15×10^{-9} A cm^{-2}). The drastic decrease in leakage current (three orders of magnitude) for the OPD device with the active layer thickness of 80 nm insinuates the effective suppression of charge carriers injection from the electrodes by the blocking layers. The thinner active layer is prone to have a surface morphology with defects, thus generating the lower shunt resistance (R_{SH}) that contributes to the increase of leakage current as reported by Kim et al.[39] To further explore the interfacial phenomenon, impedance spectroscopic study was carried out to investigate the

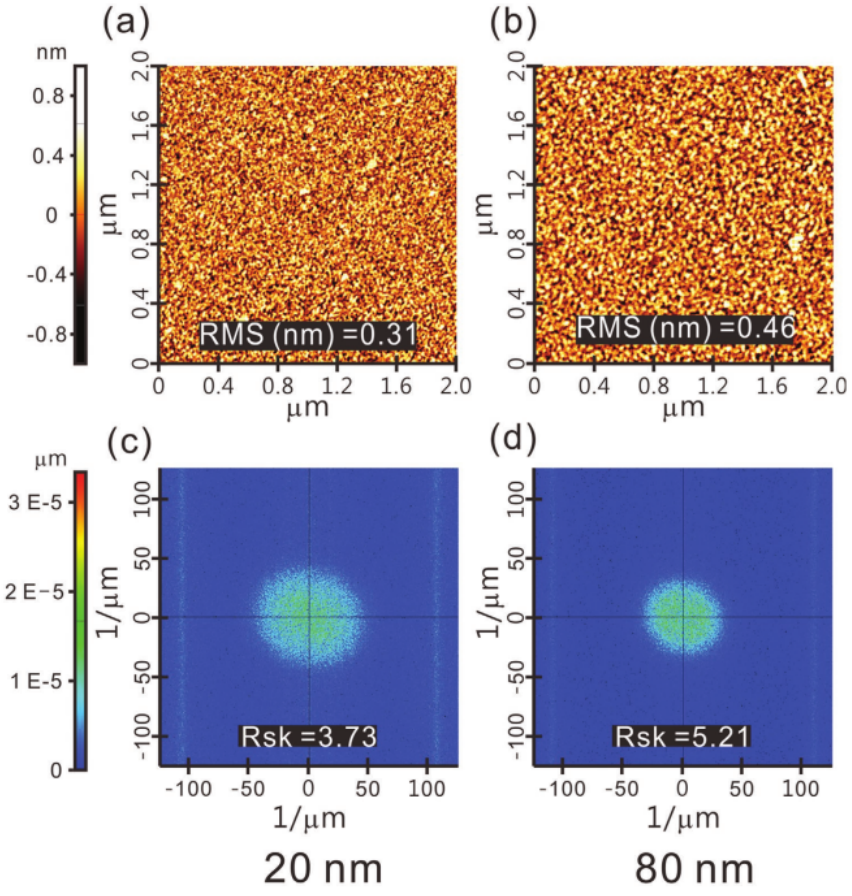

Figure 4. AFM images with parameter of RMS & Rsk for ClAlPc:C_{70} (1:3) blend with the thickness of the active layer a,c) 20 nm and b,d) 80 nm.

charge transfer resistance in bulk heterojunction.[12,40–42] In the dark condition, the Nyquist plot shows comparatively lower charge transfer resistance (R_{CT}) for the device with the active layer thickness of 20 nm under an AC signal (Figure S2a, Supporting Information).[12,40] In addition, the device with the active layer thickness of 20 nm shows the lowest constant phase element, i.e., less capability of storing the charge.[40,42] Under illumination condition, the OPD device employing the active layer with the respective thickness of 20, 40, 60, and 80 nm exhibited the photocurrent density (J_{ph}) of 6.63, 13.55, 16.46, and 16.02 mA cm^{-2}, respectively. The slight decrease in the photocurrent density for the active layer thickness of 80 nm compared to that of the device with 60 nm active layer is attributed to the lattice polarization that reduces the carrier diffusion and recombination.[40]

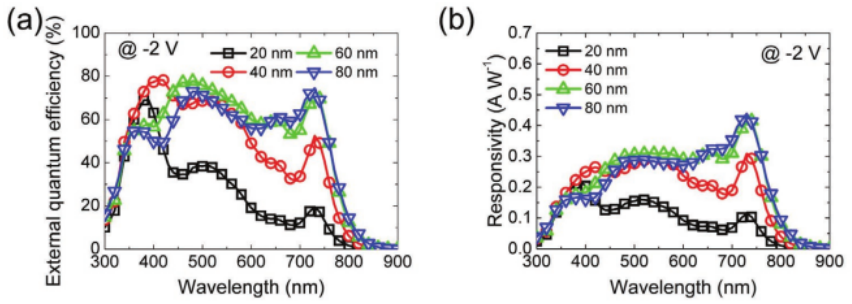

Figure 5. The spectral response of the OPD device with various active layer thickness under a bias voltage of −2 V. a) External quantum efficiency and b) responsivity.

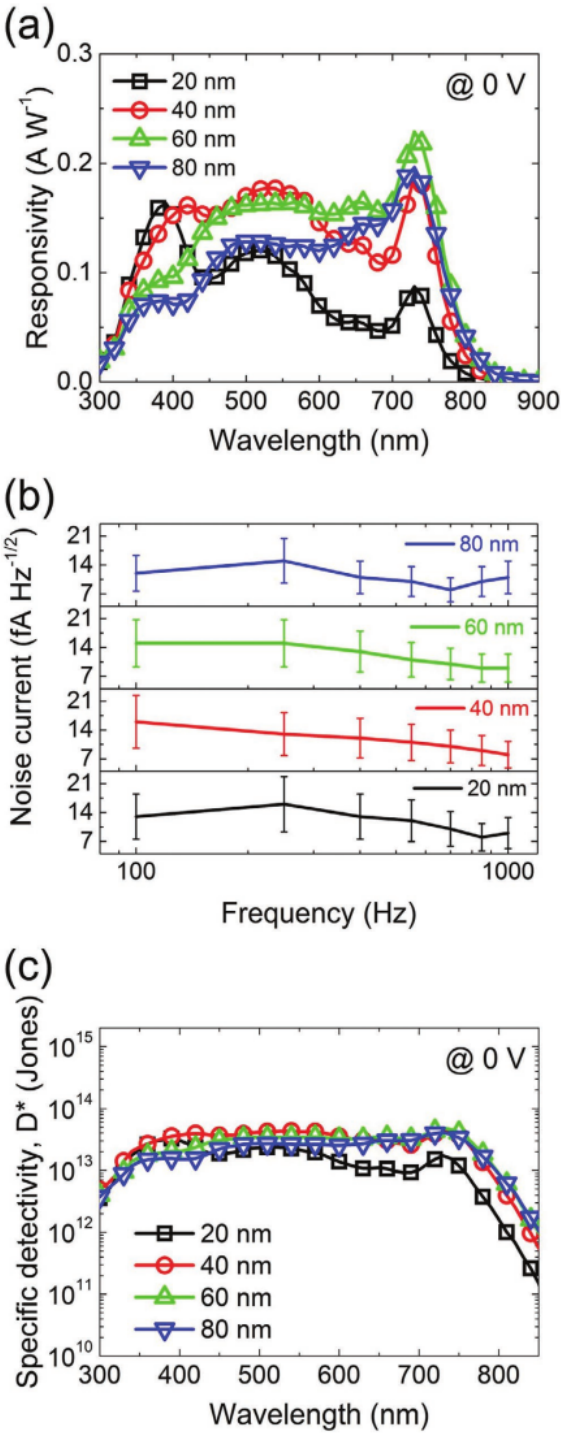

Figure 6. a) Responsivity, b) noise current, and c) specific detectivity of the OPD device with various active layer thicknesses by applying the zero bias voltage.

The surface morphologies of the active layers with thicknesses of 20 and 80 nm were analyzed by atomic force microscope (AFM) and are displayed as the images in **Figure 4** for comparison. The high value of roughness (RMS) and skewness (Rsk) of the active layer with the thickness of 80 nm compared to 20 nm or other thickness (see Figure S3 (Supporting Information) for 40 and 60 nm) are resulted from the higher density of grains.[43,44] Moreover, Figure 4c,d shows the 2D fast Fourier transform (2D-FFT) of the corresponding AFM images depicting the symmetry of the respective surface morphologies.[45,46] The EQE spectra (**Figure 5**a) are similar for all the OPD devices with different thicknesses of the active layer. Meanwhile, the EQE increases according to the active layer thickness irrespective of the wavelengths, suggesting higher optical absorption and charge generation in the thicker bulk heterojunction.[19,47] To address such phenomena, the EQE spectra (see Figure S4, Supporting Information) were normalized. The normalized EQE demonstrates a similar trend to the optical distribution in the device, and the results indicate that the cavity effect contributes to the photogeneration carrier profile and thus gradually improves the response in the NIR region (at the wavelength of 730 nm). However, the EQE at the wavelength range of 350–450 nm does not follow the trend as mentioned above, where the EQE peak is higher for the active layer with a thickness of 40 nm. This phenomenon could be attributed to the cumulative result of the optical cavity effect related to the optimized thickness of the active layer as well as the reduction in trap-assisted recombination due to the larger grain sizes in the thicker active layers.[22,39,47,48] As expected, the responsivity of OPD devices (see Figure 5b) also follows a similar trend as EQE data. The OPD device with the active layer thickness of 80 nm shows the highest EQE and responsivity of 74.6% and 0.439 A W^{-1}, respectively, at the wavelength of 730 nm under a bias of −2 V, while an active layer thickness of 60 nm outperforms slightly in the wavelength range of 350 to 450 nm (see Table S1 for details, Supporting Information).

Specific detectivity, D^*, of a photodetector determines its ability to detect the weakest photosignal under various noises such as shot, Johnson (thermal), and flicker (1/f).[12,19,22,49–54] D^* is a crucial figure of merit for photodetectors, which is usually expressed in the simple equation by[8–18,21,22,38,52,54,55]

$$D^* = \frac{R}{\sqrt{2\,q\,J_{\text{dark}}}} \tag{1}$$

where R is the responsivity (A W^{-1}), q is elementary charge (1.6×10^{-19} C), and J_{dark} is dark current density (A cm^{-2}). In principle, J_{dark} is the sum of total noise, including the shot noise, thermal (Johnson) noise, and flicker noise (1/f). Generally, the flicker noise is negligible at frequencies beyond 100 Hz[51] while the shot noise (i_{shot}) and thermal noise (i_{thermal}) could be estimated by following[52]

$$i_{\text{shot}} = \sqrt{2\,q\,I_{\text{dark}}\,B} \tag{2}$$

$$i_{\text{thermal}} = \sqrt{\frac{4\,k\,T\,B}{R_{\text{SH}}}} \tag{3}$$

where I_{dark} is dark current (Ampere), B is normalized bandwidth (value in 1), k is Boltzmann constant (1.38×10^{-23} J K^{-1}),

Table 1. The characteristics of OPD devices with various thickness of the active layer based on ClAlPc:C_{70} blend. The average (avg) value is calculated by eight devices for each recipe of the OPD.

Active layer thickness [nm]	Dark current density [A cm^{-2}] [a]		EQE [%] [b]		R [A W^{-1}] [c]		i_{noise} [fA Hz$^{-1/2}$] [d]	D^* [Jones] [e]
	Avg	Min	Avg	Max	Avg	Max		
20	6.05×10^{-6}	5.90×10^{-6}	17.7	19.5	0.079	0.087	16.00 ± 6.72	1.72×10^{13}
40	1.61×10^{-8}	1.48×10^{-8}	51.9	52.5	0.188	0.189	13.00 ± 5.20	4.61×10^{13}
60	1.89×10^{-9}	1.66×10^{-9}	73.2	73.6	0.227	0.229	15.00 ± 5.70	4.82×10^{13}
80	1.29×10^{-9}	1.15×10^{-9}	73.2	74.6	0.193	0.196	15.00 ± 5.40	4.14×10^{13}

[a]The values are based on measurement at the point of a reverse bias voltage of −2 V; [b]The spectral responses are based on measurement using a reverse bias voltage of −2 V with the peak detection values at a wavelength radiance of 730 nm; [c]The spectral responses are based on measurement under zero bias voltage with the peak detection values at a wavelength radiance of 730 nm; [d]The values are based on measurement under zero bias voltage; [e]The values are derived from Equation (4), where $A = 0.04$ cm^2 and $f = 250$ Hz.

T is the temperature in Kelvin, R_{SH} is shunt resistance measured by impedance spectroscopy following Nyquist theory (see Figure S2a, Supporting Information). Here, there has already knew some limitations to adopt Equation (1) for the calculation of D^*. For example, Equation (1) assumes that the total noises of the photodetector are dominated by shot noise in I_{dark}, which means that the shot noise level must be several times or even an order of magnitude higher than that of the Johnson (thermal) noise.[52] The R_{SH} of proposed OPDs with active layer thicknesses of 20, 40, 60, and 80 nm are 0.78, 1.18, 1.23, and 1.47 MΩ, respectively. Based on the results of I_{dark} and R_{SH}, the calculated i_{shot} near zero bias shows twice of magnitude lower than the thermal noise (see Table S1, Supporting Information). Therefore, it is not reasonable to utilize Equation (1) for estimating D^*. Besides, we observed similar behavior of polymer photodetectors in other works,[51,55] implying that the equation for D^* should be used as following[51,53–55]

$$D^* = \frac{R\sqrt{A\,f}}{i_{noise}} \tag{4}$$

where R is the responsivity (A W^{-1}), A is detection area (cm^{-2}), f is the bandwidth (Hz), and i_{noise} is the noise current (A Hz$^{-1/2}$). The noise current of photodetector can be measured by a lock-in amplifier in current measurement mode.[53] According to Equation (4), **Figure 6**a–c provides the results of responsivity, noise current, and D^*. The level of the noise current for our OPDs is closed to a few fA Hz$^{-1/2}$, which results in the D^* of 1.72×10^{13}, 4.61×10^{13}, 4.82×10^{13}, and 4.14×10^{13} cm Hz$^{1/2}$ W^{-1} with the active layer thickness

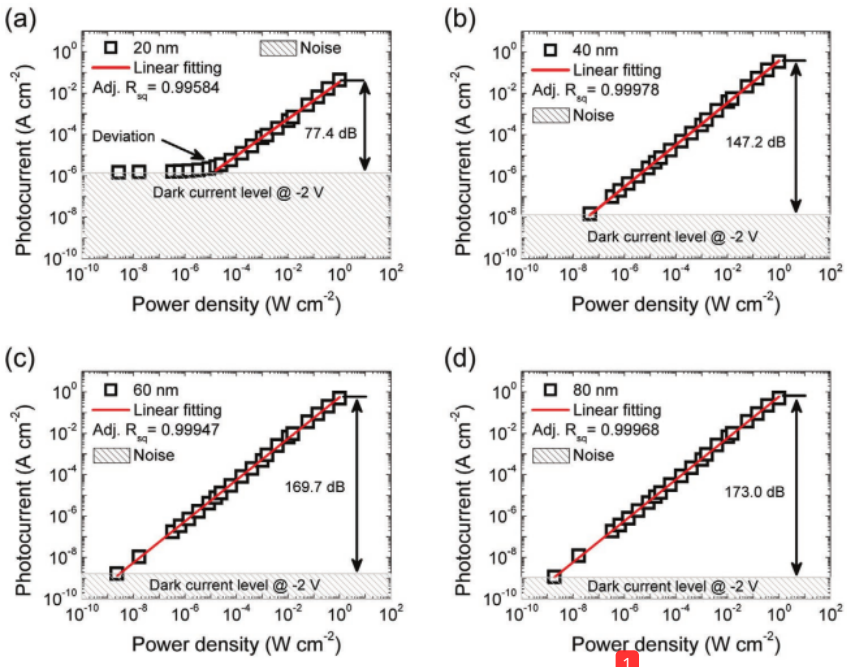

Figure 7. The LDR measurement of the OPD device at a bias of −2 V under a 780 nm radiant flux from 1 W cm^{-2} to 1 nW cm^{-2} with the active layer thickness of a) 20 nm, b) 40 nm, c) 60 nm, and d) 80 nm. The Adj. R_{sq} value is the mean square deviation from the linear fitting results.

Table 2. The summary of dynamic characteristics of OPD devices with various thickness of the active layer based on ClAlPc:C_{70} blend.

Active layer thickness [nm]	Resistance [Ω] [a)]	Capacitance [nF] [a)]	$f_{RC,-3dB}$ [kHz] [b)]	f_{-3dB} [kHz] [c)]	Rise time [µs] [d)]	Fall time [µs] [d)]
20	110.60 ± 4.88	4.941 ± 0.091	291.2	105.5	5.97	6.26
40	85.18 ± 4.20	3.222 ± 0.043	579.9	526.9	7.85	4.45
60	85.44 ± 3.33	2.413 ± 0.023	772.0	730.9	4.69	0.87
80	100.80 ± 4.30	1.908 ± 0.021	827.5	778.7	2.13	0.77

[a)]The values based on the fitting result of equivalent circuit, measured by Solartron analytical Materials Lab XM under illumination of 780 nm LED light with a flux density of 1 mW cm^{-2}; [b)]The frequency response calculation values are based on Equation (7); [c)]The values are based on measurement from trigger of 780 nm LED light with a flux density of 1 mW cm^{-2}, monitored by oscilloscope; [d)]The record of transient photovoltage response values at a pulse frequency of 10 kHz from trigger of 780 nm LED light with a flux density of 1 mW cm^{-2}.

of 20, 40, 60, and 80 nm, respectively (Figure 6c). The details of the calculation are summarized in **Table 1**. In addition, the data of responsivity and specific detectivity are summarized in Table S2 (Supporting Information), at the wavelengths of 370, 530, and 730 nm with the active layer employing the different thicknesses.

The response of the OPD device under various intensities of light was studied by measuring the linear dynamic range (LDR), which is expressed as the ratio of the strongest to the weakest optical power (irradiance) when the device maintains its linear response.[20,49] **Figure 7** depicts the LDR plots of the OPD devices which are exposed to radiance from laser and LED at a bias voltage of −2 V. The LDR (dB) of OPD device was calculated by using Equation (5)[5,14,15,20–22,31,52,55,56]

$$\mathrm{LDR} = 20 \log\left(\frac{J_{\max(V)}}{J_{\min(V)}}\right) \tag{5}$$

here $J_{max(V)}$ and $J_{min(V)}$ are the maximum and minimum of the detectable photocurrent density (A cm^{-2}) with applying a similar bias voltage. The OPD device with the active layer thicknesses of 20, 40, 60, and 80 nm achieved the LDR values of 77.4, 147.2, 169.7, and 173.0 dB, respectively (Table S3, Supporting Information), indicating the linear correlation. The OPD device with an active layer thickness of 20 nm shows comparatively low LDR with much faster deviation from the linearity at low optical power, which could be attributed to the shot noise caused by the large leakage current (or high dark current density) and the low photocurrent, also the flicker noise caused by trap states at low frequency.[5,19] It is worthy to mention that the LDR of the OPD devices increases at 0 V bias, which can be attributed to the extremely low dark current density. Meanwhile, the photocurrent density gets saturated at high illumination due to the direct recombination of free carriers (bimolecular recombination), which governs the limit of the upper dynamic range (Figure S5, Supporting Information).[5,14,19] Based on Equation (5), the LDR values exhibited by the OPD devices under this study are higher compared to ClInPc (77.2 dB) which is a similar derivative of ClAlPc as well as other organic-based OPDs from previous reports[31] and considerably similar to organic-inorganic hybrid perovskite photodetectors (191 dB),[56] notwithstanding lower than inorganic Si photodetectors (200–240 dB).[17]

The performance of the OPD device was further investigated by studying the frequency response and transient photovoltage. The frequency bandwidth of the OPD device was estimated by measuring the cut-off frequency (f_{-3dB}) at the signal strength of −3dB under continuous illumination.[14,15,20] Fundamentally, f_{-3dB} of an OPD device is expressed in terms of the transport time of charge carriers and the time constant (RC) following Equation (6)[5,20–22,56]

$$\frac{1}{f_{-3dB}^2} = (2\pi R_{tot} C)^2 + \left(\frac{2\pi t_{tr}}{3.5}\right)^2 \tag{6}$$

where R_{tot} is the total series resistance (ohm, including the measuring instrument), C is the capacitance (Farad), and t_{tr} is the transport time (second) of charge carriers. However, the previous work by Lee et al. demonstrated that a large device area showed the limitation of the bandwidth in frequency response (f_{-3dB}). Therefore the RC-controlled frequency response ($f_{RC,-3dB}$) of the OPD could be expressed as[21]

$$f_{RC,-3dB} = \frac{1}{2\pi R C} \tag{7}$$

where R is the series resistance (ohm) and C is the capacitance (Farad). According to the equivalent circuit measurements, the critical parameters can be readily obtained, i.e., the values of series resistance and capacitance for the OPDs with different thicknesses of the active layer, as shown in **Table 2**. According to the equivalent circuit, the value of capacitance decreases monotonically with the increase in the thickness of the active layers. This may imply that a thicker active layer can improve the photoresponse time of OPDs. The values of the cut-off frequency of the OPD device are improved from 105.5 to 778.7 kHz by varying the active layer thickness from 20 to 80 nm as depicted in **Figure 8**a. As shown in Table 2, both the frequency response of $f_{RC,-3dB}$ (from the RC-based measurement) and f_{-3dB} (from the oscilloscope-based measurement) indicate that a thicker active layer is responsible to the longer diffusion of the charge carriers and shallow trap states.[12,39,48]

Hence, the transient photovoltage of an OPD device is directly related to the transport time of charge carriers collected at the electrodes, which provides information on the response time of the OPD device measured in the form of the rise time and fall time.[14,15,21,22] Here, the rise and fall time is respectively defined as the time interval for the photovoltage reaching from 10% up to 90% and 90% down to 10% of its maximum value measured from the response under modulated-illumination.[13–15,19,49,50] Based on the trigger pulse in a frequency of 10 kHz, the transient photovoltage of OPD device was recorded

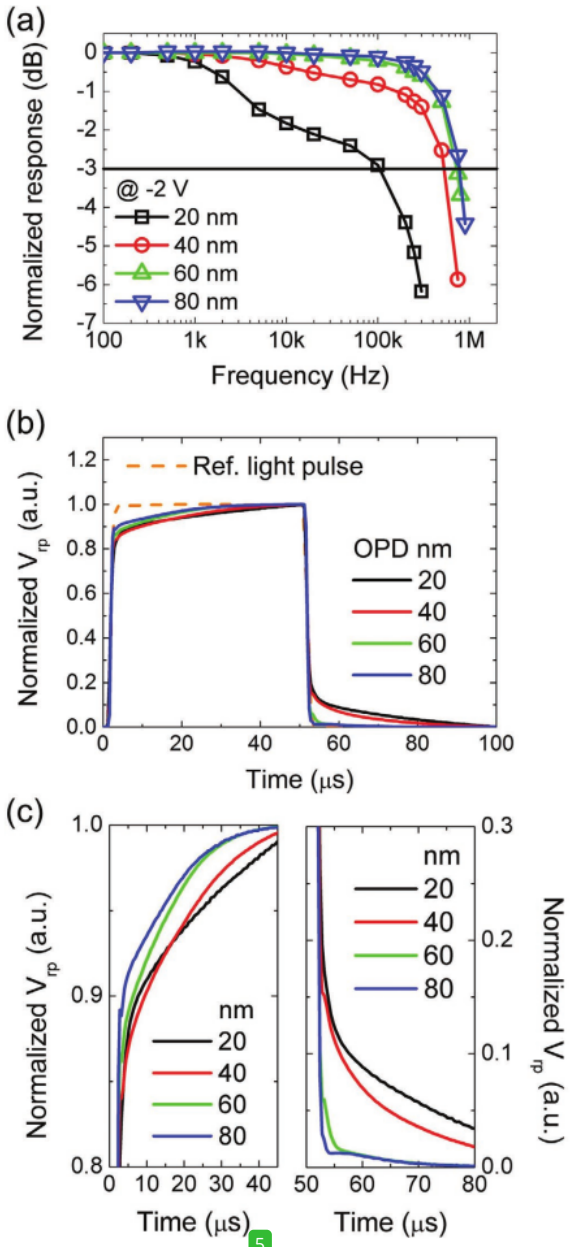

Figure 8. The response speed of the OPD devices at a bias voltage of –2 V under 1 mW cm^{-2} 780 nm illumination with modulated frequency. a) Normalized bandwidth of frequency response, b) normalized square waveform of transient photovoltage. The reference light signal is also included as the dashed line for a comparison. c) Rise and fall time from the normalized pulse of transient photovoltage.

as shown in Figure 8b. The device with an active layer thickness of 40 nm exhibits a shorter rise time as compared to that of the device with an active layer thickness of 20 nm as seen clearly in Figure 8c. Such effect is also clearly visible in Figure S2b (Supporting Information) with the presence of R_{CT} at the second semi-circle representing shunt resistance.[41] However, the inset in Figure S2b (Supporting Information) zooms in the first semi-circle of the Nyquist plot depicting the carrier diffusion pathways in the devices with the active layer thickness of 20 and 40 nm, thereby the corresponding RC time.[57] The detail information related to the photodynamic response for all the OPD devices are summarized in Table 2. To investigate the operational stability/lifetime of our OPD, the method of the light-aging (power density of ≈1 mW cm^{-2}) was utilized to evaluate the device performance as shown in Figure S6 (Supporting Information). The current density of the OPDs under continuous light-soaking showed a very stable profile keeping almost the constant value for one week. This result implies that our OPDs may have a good potential in wearable sensing applications.

3. Conclusion

This study has demonstrated a systematic and comprehensive investigation on an efficient small molecule-based photodetector with a steady wavelength responding to the region of NIR, which was successfully achieved by tuning the thickness of the active layer. The active blend comprising ClAlPc as donor and C_{70} as acceptor together with the introduction of carrier-blocking layers, TAPC:10% MoO_3 and BPhen, for effectively suppressing the leakage current. Moreover, the classical figures of merit, such as quantum yield, responsivity, specific detectivity, linear dynamic range, cut-off frequency, and response time, were further investigated and interpreted by absorbance spectra, AFM topography, and impedance spectroscopy. The optimal OPD device reported in this work responds strongly at the wavelength of 730 nm with the dark current density of 1.15 × 10^{-9} A cm^{-2} and EQE of 74.6% accompanied by the responsivity of 0.439 A W^{-1}, the LDR of 173 dB, and the frequency response of 778.7 kHz along with rise/fall time of 2.13/0.77 μs (based on trigger pulses at a frequency of 10 kHz) under a reverse bias voltage of –2 V, while the specific detectivity of 4.14 × 10^{13} cm Hz$^{1/2}$ W^{-1} at zero bias voltage. Our results suggest the possible applicability of this NIR active OPD device as a receiver in optical communications.[58]

4. Experimental Section

The materials such as TAPC (>98%), MoO_3 (>99%), ClAlPc (85%), fullerene (C_{70}, >98%), 4,7-diphenyl-1,10-phenanthroline (BPhen, >99%), and Ag were purchased from Merck KGaA (Sigma-Aldrich). All the organic materials were purified once (twice for ClAlPc) in homemade temperature gradient sublimation system before vacuum-deposited on commercially available ITO-coated glass substrates (Luminescence Technology Corp., 15 ohm sq^{-1}) to fabricate the sequential layers. The OPD device with the structure of ITO/TAPC:10% MoO_3 (30 nm)/ClAlPc:C_{70} (1:3; with 20, 40, 60, and 80 nm thicknesses)/BPhen (3 nm)/Ag (90 nm) and active area of 4 mm^2 were fabricated in the thermal evaporation chamber at 2 × 10^{-6} Torr and the deposition rate of 0.5–1 Å s^{-1} (3 Å s^{-1} for Ag deposition). The thickness of each layer was measured by the quartz crystal microbalance, which was calibrated by a surface profiler (Bruker, DektakXT). The final devices were encapsulated in a nitrogen-filled glove box (O_2 < 0.1 ppm;

H_2O < 0.1 ppm) by attaching a glass substrate with UV-curable epoxy resin under UV illumination.

The absorption coefficient spectra of the organic thin-films for the material of donor (D) ClAlPc and acceptor (A) C_{70}, on a quartz substrate was recorded using UV–vis spectrophotometer (Jasco, V-770) and the morphology of the layer (2 μm × 2 μm) on a silicon substrate was studied by atomic force microscope (AFM) (Park Systems, XE-70) in noncontact mode with a silicon tip (PPP-NCHR). All the electro-optical measurements of the OPD devices encapsulated with glass substrates were performed in the ambient atmosphere (room temperature of ≈26 °C; humidity of ≈50%). The current density–voltage (J–V) characteristics of OPDs were measured using a programmable source meter (Keithley, model 2636A) in the dark condition and under one sun solar simulator (Newport, 91160A) with an intensity of 100 mW cm^{-2}. The resistive and capacitive properties of the OPDs were investigated by impedance spectroscopy (Solartron, Materials Lab XM) with a sinusoidal AC signal (under an amplitude of ≈500 mV) tuned in the frequency range from 10^{-6} to 1 MHz. Noise current was directly measured from SR830 lock-in amplifier. To measure the EQE and responsivity of OPDs, monochromatic light beams from a commercial light source (Newport, TLS-300XR) calibrated with Si photodetector (Newport, 818-UV) were chopped at the frequency of 250 Hz by an optical chopper system before it was illuminated on the devices and the response was recorded by a lock-in amplifier (Signal Recovery 7225), while the details of the spectral radiance are presented in Figure S7 (Supporting Information). For measurement of LDR, the emission wavelengths of 785 and 780 nm from respective light beam of laser (CNI, MLL-III-785) and LED (Thorlabs, M780L3) were directing to motorized filter wheel (Thorlabs, FW102CNEB), then its radiances were used to irradiance the area of OPDs device. In the measurement of frequency response and transient photovoltage, the light beam from commercially LED (Thorlabs, the emission wavelength of 780 nm) with a flux density of 1 mW cm^{-2} that generated from a function generator (Tektronix, AFG3102C) was triggering the response of OPDs device; hereafter the response of signal was converted from photocurrent to photovoltage by the low noise current preamplifier with an A/V gain factor of 10^5 and without any bandwidth filters (Ametek, model 5182), then it was displayed and recorded using 2.5 GHz oscilloscope (Teledyne LeCroy, WaveRunner 625Zi). Moreover, an LED light with a flux density of 1.01 mW cm^{-2} (Thorlabs; MWWHLP1 3000 K) was used for the stability/lifetime measurement, where the power density was recorded by the spectrum meter (Optimum, SRI-2000).

Supporting Information

Supporting Information is available from the Wiley Online Library or from the author.

Acknowledgements

R.E. and Y.-Z.L. contributed equally to this study. The authors acknowledge financial support from the Ministry of Science and Technology (Grant Nos. MOST 107-2113-M-002-019-MY3, 107-2221-E-131-029-MY2, 107-2119-M-131-001, 108-2221-E-131-027-MY2, and 108-2221-E-011-151) and industry project from the Central Taiwan Science Park (108RB04). S.-W.L. is grateful to H.-H. Wu, Syskey Technology Co., Ltd. (Taiwan), for his assistance in designing the fabrication system. Also, the authors thank Maya Angela for helping to prepare the picture for ToC.

Conflict of Interest

The authors declare no conflict of interest.

Keywords

blocking layers, chloroaluminium phthalocyanine, fullerene, near-infrared photodetectors, small molecules

Received: March 25, 2020
Revised: May 28, 2020
Published online:

[1] K. Walzer, B. Maennig, M. Pfeiffer, K. Leo, *Chem. Rev.* **2007**, *107*, 1233.
[2] S.-W. Liu, Y.-Z. Li, S.-Y. Lin, Y.-H. Li, C.-C. Lee, *Org. Electron.* **2016**, *30*, 275.
[3] Z. Su, F. Hou, X. Wang, Y. Gao, F. Jin, G. Zhang, Y. Li, L. Zhang, B. Chu, W. Li, *ACS Appl. Mater. Interfaces* **2015**, *7*, 2529.
[4] S.-W. Liu, C.-C. Lee, C.-H. Yuan, W.-C. Su, S.-Y. Lin, W.-C. Chang, B.-Y. Huang, C.-F. Lin, Y.-Z. Lee, T.-H. Su, K.-T. Chen, *Adv. Mater.* **2015**, *27*, 1217.
[5] A. Armin, M. Hambsch, I. K. Kim, P. L. Burn, P. Meredith, E. B. Namdas, *Laser Photonics Rev.* **2014**, *8*, 924.
[6] M. Ichikawa, T. Takeuchi, H.-G. Jeon, Y. Jin, S. Lee, K.-S. Kim, *Jpn. J. Appl. Phys.* **2012**, *51*, 34103.
[7] M.-S. Choi, S. Lee, H. J. Kim, J.-J. Kim, *Org. Electron.* **2018**, *61*, 164.
[8] J. B. Wang, W. L. Li, B. Chu, C. S. Lee, Z. S. Su, G. Zhang, S. H. Wu, F. Yan, *Org. Electron.* **2011**, *12*, 34.
[9] X. Wang, H. Li, Z. Su, F. Fang, G. Zhang, J. Wang, B. Chu, X. Fang, Z. Wei, B. Li, W. Li, *Org. Electron.* **2014**, *15*, 2367.
[10] W. Lv, Y. Peng, J. Zhong, X. Luo, Y. Li, T. Zheng, Y. Tang, L. Du, L. Peng, *IEEE Photonics Technol. Lett.* **2015**, *27*, 2043.
[11] K.-J. Baeg, M. Binda, D. Natali, M. Caironi, Y.-Y. Noh, *Adv. Mater.* **2013**, *25*, 4267.
[12] Z. Wu, Y. Zhai, H. Kim, J. D. Azoulay, T. N. Ng, *Acc. Chem. Res.* **2018**, *51*, 3144.
[13] M. Kielar, O. Dhez, L. Hirsch, *Proc. SPIE* **2016**, *9944*, 994409.
[14] M. Kielar, O. Dhez, G. Pecastaings, A. Curutchet, L. Hirsch, *Sci. Rep.* **2016**, *6*, 39201.
[15] X. Liu, Y. Lin, Y. Liao, J. Wu, Y. Zheng, *J. Mater. Chem. C* **2018**, *6*, 3499.
[16] J. Miao, F. Zhang, Y. Lin, W. Wang, M. Gao, L. Li, J. Zhang, X. Zhan, *Adv. Opt. Mater.* **2016**, *4*, 1711.
[17] M. Wang, Y.-Z. Li, H.-C. Chen, C.-W. Liu, Y.-S. Chen, Y.-C. Lo, C.-S. Tsao, Y.-C. Huang, S.-W. Liu, K.-T. Wong, B. Hu, *Mater. Horiz.* **2020**, *7*, 1171.
[18] S. Yoon, J. Ha, K. M. Sim, W. Cho, D. S. Chung, *Org. Electron.* **2016**, *35*, 17.
[19] D. Yang, D. Ma, *Adv. Opt. Mater.* **2019**, *7*, 1800522.
[20] S. Yoon, K. M. Sim, D. S. Chung, *J. Mater. Chem. C* **2018**, *6*, 13084.
[21] C.-C. Lee, S. Biring, S.-J. Ren, Y.-Z. Li, M.-Z. Li, N. R. Al Amin, S.-W. Liu, *Org. Electron.* **2019**, *65*, 150.
[22] N. Strobel, R. Eckstein, J. Lehr, U. Lemmer, G. Hernandez-Sosa, *Adv. Electron. Mater.* **2018**, *4*, 1700345.
[23] V. Pecunia, *J. Phys. Mater.* **2019**, *2*, 042001.
[24] H. Sun, T. Liu, J. Yu, T.-K. Lau, G. Zhang, Y. Zhang, M. Su, Y. Tang, R. Ma, B. Liu, J. Liang, K. Feng, X. Lu, X. Guo, F. Gao, H. Yan, *Energy Environ. Sci.* **2019**, *12*, 3328.
[25] C. Wang, X. Chen, F. Chen, J. Shao, *Org. Electron.* **2019**, *66*, 183.
[26] Y. Higashi, K.-S. Kim, H.-G. Jeon, M. Ichikawa, *J. Appl. Phys.* **2010**, *108*, 034502.
[27] C.-C. Lee, W.-C. Su, Y.-S. Shu, W.-C. Chang, B.-Y. Huang, Y.-Z. Lee, T.-H. Su, K.-T. Chen, S.-W. Liu, *RSC Adv.* **2015**, *5*, 5617.
[28] M.-S. Choi, S. Chae, H. J. Kim, J.-J. Kim, *ACS Appl. Mater. Interfaces* **2018**, *10*, 25614.
[29] T. Zhao, G. Zhang, Y. Xing, *RSC Adv.* **2018**, *8*, 10999.

[30] R. Pandey, R. A. Kerner, S. M. Menke, J. Holst, K. V. B. Josyula, R. J. Holmes, *Org. Electron.* **2013**, *14*, 804.
[31] C. W. Joo, J. Kim, J. Moon, K. M. Lee, J.-E. Pi, S.-Y. Kang, S.-D. Ahn, Y.-S. Park, D. S. Chung, *Org. Electron.* **2019**, *70*, 101.
[32] R. F. Bailey-Salzman, B. P. Rand, S. R. Forrest, *Appl. Phys. Lett.* **2007**, *91*, 013508.
[33] M. S. Roy, P. Balraju, Y. S. Deol, S. K. Sharma, G. D. Sharma, *J. Mater. Sci.* **2008**, *43*, 5551.
[34] K. Harada, T. Edura, C. Adachi, *Appl. Phys. Express* **2010**, *3*, 121602.
[35] J. H. Lee, C.-H. Chen, C.-L. Lin, S.-P. Yang, T.-L. Chiu, *J. Photonics Energy* **2018**, *8*, 045502.
[36] L. Du, X. Luo, F. Zhao, W. Lv, J. Zhang, Y. Peng, Y. Tang, Y. Wang, *Carbon* **2016**, *96*, 685.
[37] D. Natali, M. Caironi, in *Photodetectors: Materials, Devices and Applications* (Ed.: B. Nabet), Woodhead Publishing, Sawston, UK **2016**, pp. 195–254.
[38] S. Shafian, H. Hwang, K. Kim, *Opt. Express* **2016**, *24*, 25308.
[39] H. Kim, K.-T. Lee, C. Zhao, L. J. Guo, J. Kanicki, *Org. Electron.* **2015**, *20*, 103.
[40] E. Von Hauff, *J. Phys. Chem. C* **2019**, *123*, 11329.
[41] K. Park, J. Xi, Q. Zhang, G. Cao, *J. Phys. Chem. C* **2011**, *115*, 20992.
[42] D. B. Patel, K. R. Chauhan, I. Mukhopadhyay, *Phys. Chem. Chem. Phys.* **2014**, *16*, 20900.
[43] F. M. Mwema, O. P. Oladijo, T. S. Sathiaraj, E. T. Akinlabi, *Mater. Res. Express* **2018**, *5*, 046416.
[44] E. S. Gadelmawla, M. M. Koura, T. M. A. Maksoud, I. M. Elewa, H. H. Soliman, *J. Mater. Process. Technol.* **2002**, *123*, 133.
[45] H.-G. Park, H.-C. Jeong, Y. H. Jung, D.-S. Seo, *Sci. Rep.* **2015**, *5*, 12356.
[46] J. S. Bangsund, T. R. Fielitz, T. J. Steiner, K. Shi, J. R. Van Sambeek, C. P. Clark, R. J. Holmes, *Nat. Mater.* **2019**, *18*, 725.
[47] A. Armin, M. Velusamy, P. Wolfer, Y. Zhang, P. L. Burn, P. Meredith, A. Pivrikas, *ACS Photonics* **2014**, *1*, 173.
[48] W. L. Leong, S. R. Cowan, A. J. Heeger, *Adv. Energy Mater.* **2011**, *1*, 517.
[49] A. K. Maini, *Handbook of Defence Electronics and Optronics: Fundamentals, Technologies and Systems*, John Wiley & Sons Ltd, Chichester, UK 2018.
[50] L. B. Stotts, *Free Space Optical Systems Engineering: Design and Analysis*, John Wiley & Sons, Inc., Hoboken, New Jersey **2017**.
[51] Z. Wu, W. Yao, A. E. London, J. D. Azoulay, T. N. Ng, *Adv. Funct. Mater.* **2018**, *28*, 1800391.
[52] Z. Lan, Y. Lei, W. K. E. Chan, S. Chen, D. Luo, F. Zhu, *Sci. Adv.* **2020**, *6*, eaaw8065.
[53] H. L. Zhu, Z. Liang, Z. Huo, W. K. Ng, J. Mao, K. S. Wong, W.-J. Yin, W. C. H. Choy, *Adv. Funct. Mater.* **2018**, *28*, 1706068.
[54] Z. Zhong, L. Bu, P. Zhu, T. Xiao, B. Fan, L. Ying, G. Lu, G. Yu, F. Huang, Y. Cao, *ACS Appl. Mater. Interfaces* **2019**, *11*, 8350.
[55] Z. Zhong, K. Li, J. Zhang, L. Ying, R. Xie, G. Yu, F. Huang, Y. Cao, *ACS Appl. Mater. Interfaces* **2019**, *11*, 14208.
[56] C. Li, H. Wang, F. Wang, T. Li, M. Xu, H. Wang, Z. Wang, X. Zhan, W. Hu, L. Shen, *Light: Sci. Appl.* **2020**, *9*, 31.
[57] A. Fakharuddin, I. Ahmed, Z. Khalidin, M. M. Yusoff, R. Jose, *J. Appl. Phys.* **2014**, *115*, 164509.
[58] I. Tavakkolnia, M. D. Soltani, M. A. Arfaoui, A. Ghrayeb, C. Assi, M. Safari, H. Haas, in *2019 IEEE Int. Conf. Commun. Workshops (ICC Workshops 2019) – Proceedings*, IEEE, Shanghai, China **2019**, 8757144.

Vacuum-Processed Small Molecule Organic Photodetectors with Low Dark Current Density and Strong Response to Near-Infrared Wavelength

ORIGINALITY REPORT

7%	8%	8%	1%
SIMILARITY INDEX	INTERNET SOURCES	PUBLICATIONS	STUDENT PAPERS

PRIMARY SOURCES

1	pubs.rsc.org Internet Source	3%
2	Min-Soo Choi, Sangmin Chae, Hyo Jung Kim, Jang-Joo Kim. " Control of Crystallinity in PbPc:C Blend Film and Application for Inverted Near-Infrared Organic Photodetector ", ACS Applied Materials & Interfaces, 2018 Publication	1%
3	Nurul Ridho Al Amin, Kiran Kishore Kesavan, Sajal Biring, Chih-Chien Lee, Tzu-Hung Yeh, Tzu-Yu Ko, Shun-Wei Liu, Ken-Tsung Wong. "A Comparative Study via Photophysical and Electrical Characterizations on Interfacial and Bulk Exciplex-Forming Systems for Efficient Organic Light-Emitting Diodes", ACS Applied Electronic Materials, 2020 Publication	1%
4	Chunhui Duan, Fei Huang, Yong Cao. "Solution processed thick film organic solar cells",	1%

	Polymer Chemistry, 2015 Publication	
5	d-nb.info Internet Source	1 %
6	catalog.lib.kyushu-u.ac.jp Internet Source	1 %

Exclude quotes	Off	Exclude matches	< 1%
Exclude bibliography	On		